The Research of Medical Science Review
ISSN: 3007-1208 & 3007-1216 Volume 3, Issue 8, 2025

STRUCTURAL AND FUNCTIONAL CONSEQUENCES OF PTGER3 VARIANTS ASSOCIATED WITH CONJUNCTIVITIS: A BIOINFORMATICS APPROACH

Moeen Zulfiqar[1], Hamna Tariq[*1], Muhammad Saleem[1], Kainat Ramzan[*2], Ali Noman[3], Haris Munir[1], Saira Ramzan[1], Ali Moazzam Qadri[1], Mehmooda Asif[1], Amina Islam[4]

[1]*Department of Molecular Biology, University of Okara, Punjab, 56300, Pakistan*
[*2]*Department of Biochemistry, Faculty of Life Sciences, University of Okara, 56300, Pakistan*
[3]*Department of Zoology, Faculty of Life Sciences, University of Okara, 56300, Pakistan*
[4]*Department of Microbiology and Molecular Genetics, University of Okara, 56300, Pakistan*

[*1]hamna.tariq@uo.edu.pk, [*2]kainat.ramzan@uo.edu.pk

DOI: https://doi.org/10.5281/zenodo.16991059

Keywords
Adenovirus; Conjunctivitis; EP3 receptor; G-protein-coupled receptor; Ocular inflammation; PTGER3; Prostaglandin E₂

Article History
Received on 25 May 2025
Accepted on 30 July 2025
Published on 26 August 2025

Copyright @Author
Corresponding Author: *
Hamna Tariq[*1]
Kainat Ramzan[*2]

Abstract

Conjunctivitis (pink eye) remains a prevalent ocular condition, with Pakistan reporting ~400,000 cases in 2023, particularly in Punjab. While infectious agents are the primary drivers, host genetic factors may modulate individual susceptibility. Prostaglandin E receptor 3 (PTGER3), encoded on chromosome 1p31.1, plays a central role in PGE₂-mediated inflammatory signaling. In this study, we present the first in silico analysis of PTGER3 single-nucleotide polymorphisms (SNPs) linked to conjunctival inflammation. Out of 27,077 SNPs retrieved from the NCBI and gnomAD databases, preliminary screening via SIFT and PolyPhen identified 51 potentially deleterious variants. Consensus analysis using 10 different bioinformatics tools further refined the list to 15 high-risk SNPs. Structural assessments by the HOPE server highlighted mutations such as C358R, E279K, and T277M, which significantly affect side-chain geometry and protein core stability. Wild-type and mutant models were constructed based on the AlphaFold-derived PE2R3_HUMAN (P43115A) structure and validated for stereochemical quality. FTSite analysis predicted key ligand-binding pockets, notably involving residues ALA148, LEU145, ILE287, THR138, and LEU299. Molecular docking was executed in PyRx using AutoDock Vina for both blind and focused searches. A panel of 12 anti-infective and anti-inflammatory compounds, including Luteolin, G-Mangostin, Ganomycin-I, and Proflavine, was docked against the wild-type and mutant PTGER3 proteins. Notably, strong binding affinities and interactions were observed for Luteolin, G-Mangostin, and Proflavine in the wild-type, while T277M, E279K, and C358R mutants displayed altered interaction profiles. The docking simulations, visualized through Discovery Studio Biovia, revealed critical hydrogen bonds and hydrophobic contacts stabilizing the ligand–protein complexes. These findings underscore the structural vulnerability of PTGER3 to specific amino acid substitutions and highlight several promising compounds for further evaluation as targeted EP3 receptor modulators in conjunctivitis treatment approaches.

INTRODUCTION

Pink eye (conjunctivitis) is a worldwide ocular condition, marked by inflammation of the conjunctiva, the transparent mucous membrane covering the white part of the eye and inner eyelid. Clinically, it manifests through redness, itching, tearing, a burning sensation, mucous or watery discharge, and sometimes blurred vision or photophobia [1, 2]. While most cases resolve without long-term effects, severe or untreated infections can impair vision or spread easily in communities. The epidemiology of conjunctivitis varies by region and season, such as viral conjunctivitis is primarily caused by adenoviruses, represents up to 75–80% of cases, and tends to surge in humid and densely populated environments [3, 4]. Bacterial conjunctivitis, often linked to *Staphylococcus aureus*, *Streptococcus pneumoniae*, or *Haemophilus influenzae*, is more prevalent in cooler months from December to April. Allergic conjunctivitis peaks in spring and summer due to seasonal allergens such as pollen. The etiology of conjunctivitis includes both environmental factors, such as climate, hygiene practices, air pollutants, and allergens, and genetic predispositions [1, 5, 6]. Moreover, conjunctivitis treatment has become increasingly challenging due to the emergence of antibiotic-resistant strains. In bacterial conjunctivitis, resistance is often associated with specific virulence genes such as *agr* and *spa* in *Staphylococcus aureus*, and *ply* and *psaA* in *Streptococcus pneumoniae*, which enhance bacterial survival and pathogenesis [7, 8].

Similarly, adenoviral proteins such as E1A alter host cell cycle regulation to favor viral replication, while herpes simplex virus (HSV) employs regulatory proteins and envelope glycoprotein gB to enhance viral gene expression and promote cell-to-cell spread. Even non-infectious forms, such as allergic conjunctivitis, are influenced by genetic predisposition [9, 10]. Certain gene variants, including IL4, PTGER3, FCER1A, and TNF-α, contribute to heightened immune responses in allergic conjunctivitis by modulating cytokine expression and immunoglobulin E (IgE) sensitivity [10, 11]. For instance, a polymorphism in the FOXP3 gene, known as rs3761548 (–3279 C/A), has been significantly associated with allergic conjunctivitis [12, 13]. Similarly, a genetic marker found in the GATA3 gene (rs1269486), particularly the GG genotype, appears more frequently in individuals suffering from allergic conjunctivitis and is associated with an intensified Th2 immune response, which plays a central role in allergy-related conditions [14]. A variant in the PTGER3 gene (rs1327464) has been implicated in severe ocular inflammation, particularly in combination with the HLA-A*allele. This genetic combination has been strongly linked to drug-induced conditions such as Stevens–Johnson syndrome (SJS), which can involve serious conjunctival complications [15].

Furthermore, the interplay of host genetics, epigenetic regulation, and lifestyle factors such as nutrition, urban exposure, and stress affects individual susceptibility and recovery patterns. This multifactorial nature underscores the need for personalized and preventive strategies in managing conjunctivitis [16]. The PTGER3 protein is a member of the G protein-coupled receptor (GPCR) superfamily, functions as a receptor for Prostaglandin E_2 (PGE_2), and is involved in mediating extracellular inflammatory signals into intracellular responses [17, 18]. PTGER3 belongs to the rhodopsin-like Class A GPCR subfamily and is composed of approximately 390 amino acids. Structurally, it is defined by a seven-transmembrane domain configuration, which enables effective signal transduction upon ligand binding. The PTGER3 gene encodes the EP3 receptor, which is located on the short arm of human chromosome 1 at cytogenetic band 1p31.1. According to the GRCh38/hg38 human genome assembly, it is annotated at NC_000001.11, residing within a genomic region involved in immune and inflammatory regulation. The gene spans approximately 80 kilobases (kb) and is structured into 10 exons and 9 introns [19]. It undergoes alternative splicing, giving rise to at least 8 known transcript variants in humans (EP3-1 through EP3-8), which differ in their N-terminal or intracellular domains, thus altering their interaction with G proteins and downstream signaling specificity [16, 20, 21].

Within the ocular system, it is prominently found in the corneal endothelium, conjunctival epithelium, ciliary body epithelium, and retinal Müller cells. It is also expressed in organs such as the kidneys, stomach, uterine smooth muscle, and specific regions of the

thalamus, underscoring its involvement in vasoregulation, immune response, smooth muscle function, and pain perception. Functionally, the binding of PGE_2 to the EP3 receptor, encoded by PTGER3, predominantly activates intracellular signaling via Gi-proteins, leading to the suppression of cyclic adenosine monophosphate (cAMP) levels [22]. This signaling cascade contributes to key inflammatory processes, including vasodilation, increased vascular permeability, tissue edema, and leukocyte infiltration, all characteristic features of conjunctival inflammation. Upon activation of the EP3 receptor enhances the local inflammatory response by promoting the release of cytokines, chemokines, and histamines. These mediators collectively intensify clinical symptoms such as ocular redness, swelling, itching, and discomfort, underscoring the pivotal role of PTGER3 in driving the pathophysiology of ocular surface inflammation [23, 24]. Despite its well-established roles in systemic inflammation, the receptor's contribution to conjunctivitis remains insufficiently characterized. The present study employs a comprehensive suite of computational approaches to evaluate the structural and functional consequences of PTGER3 gene variants. By integrating pathogenicity prediction algorithms, protein structural modeling, and molecular docking analyses, this study seeks to uncover mutation-driven mechanisms that may alter EP3 receptor dynamics in the eye. These insights have the potential to inform the development of precision-targeted anti-inflammatory therapeutics for the effective management of conjunctivitis.

1. METHODOLOGY

2.1 Download PTGER3 variant

The complete genomic sequence of the *PTGER3* gene (RefSeq ID: NC_000001.11) and its corresponding protein sequence (UniProt ID: P43115.1) were retrieved in FASTA format from the National Center for Biotechnology Information (NCBI) database (https://www.ncbi.nlm.nih.gov/gene). To obtain a comprehensive dataset of single-nucleotide polymorphisms (SNPs) associated with the gene, variant information was gathered from multiple reliable genomic databases, including dbSNP (http://www.ncbi.nlm.nih.gov/snp), Ensembl Genome Browser (http://asia.ensembl.org), and the Genome Aggregation Database (gnomAD) (https://gnomad.broadinstitute.org). This multi-source approach enabled a catalog of genetic variants for further computational assessment.

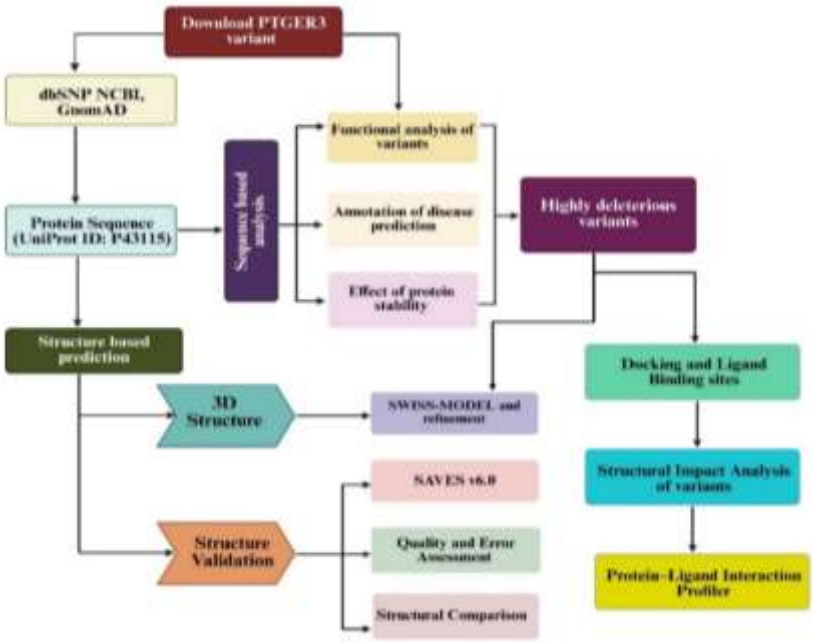


Figure 1. Flowchart of the overall computational study of the PTGER3 protein

1.2 Computational tools for Functional SNPs

To evaluate the potential functional consequences of SNPs in the PTGER3 gene, several computational tools were used in sequence. SNPnexus (https://www.snp-nexus.org/v4) provides a comprehensive annotation environment and incorporates algorithms (SIFT and PolyPhen) to determine whether a substitution is probable to affect protein function. The input can include dbSNP rsIDs or genomic coordinates [25]. PANTHER (http://pantherdb.org/tools) estimates the potential functional impact of mutations using position-specific evolutionary conservation scores. Variants located in highly conserved regions are considered more likely to disrupt protein function [26]. PolyPhen-2 (http://genetics.bwh.harvard.edu/pph2) evaluates structural and functional changes caused by amino acid substitutions. It uses homology-based modeling and position-specific scoring to predict the likelihood of a mutation being damaging, with scores closer to 1.0 indicating higher probability [27]. PredictSNP (https://loschmidt.chemi.muni.cz/predictsnp1) aggregates results from multiple tools to offer a consensus prediction. It classifies variants as either deleterious or neutral, providing a confidence score for each prediction [28, 29].

2.3 Forecast of Disease-Associated Variants

To prioritize SNPs in the PTGER3 gene with potential links to disease, three widely used computational tools were applied. Each tool offers a distinct prediction strategy based on sequence features, evolutionary conservation, and functional annotations. SNP & GO (https://snps.biofold.org/snps-and-go/snps-and-go.html) combines protein sequence information with Gene Ontology terms and evolutionary data to assess whether a variant is likely to be disease-causing. The tool provides a binary classification (disease or neutral) along with a reliability score to indicate the strength of the prediction. Meta-SNP (https://snps.biofold.org/meta-snp) functions as a meta-classifier, integrating results from several established algorithms such as SIFT, SNAP, PANTHER, and PhD-SNP. The output labels each variant as either disease-associated or neutral, offering improved accuracy through consensus-based prediction. SuSPect (http://www.sbg.bio.ic.ac.uk/suspect) uses a network-driven approach that incorporates sequence conservation, structural data, and protein–protein interaction networks. It assigns a disease susceptibility score that reflects the likelihood of each mutation contributing to pathogenic outcomes. This scoring system enables efficient prioritization of high-risk variants for further analysis [30-32].

2.4 Variations Effect on PTGER3 Protein

The i-Stable server (http://predictor.nchu.edu.tw/iStable) predicts the change in protein stability due to single-point mutations by combining outputs from multiple sequence- and structure-based algorithms. The tool provides a clear indication of whether a substitution is likely to increase or decrease protein stability, thereby aiding in identifying structurally significant variants. The MUpro tool (http://mupro.proteomics.ics.uci.edu) applies machine learning methods, including Support Vector Machines (SVM) and Neural Networks, to predict stability changes upon mutation. It processes either protein sequence or structure as input and returns a confidence-scored prediction on the stabilizing or destabilizing effect of each variant [33, 34].

2.5 Structural Impact Analysis of Variants

The structural consequences of amino acid substitutions in the PTGER3 protein were assessed using the HOPE server (https://www3.cmbi.umcn.nl/hope). This online tool analyzes the impact of point mutations by examining various features such as size, charge, and hydrophobicity differences between the wild-type and mutant residues. It also incorporates structural data, conserved regions, and functional domains to evaluate the possible effects of mutations on protein stability and function [35].

2.6 SWISS-MODEL algorithm and refinement

The initial 3D structure of the PTGER3 protein was generated using SWISS-MODEL (https://swissmodel.expasy.org), an automated homology modeling server that uses sequence-based alignments to known protein structures. The FASTA sequence of PTGER3 was submitted, and the server performed template identification, alignment, and model construction without manual intervention

[36]. To evaluate the generated model, structural parameters such as QMEAN, MolProbity, and Ramachandran plot metrics were examined, providing a preliminary assessment of model quality. Post-modeling refinement was conducted using Galaxy Refine (https://galaxy.seoklab.org/cgi-bin/submit.cgi?type=REFINE), a server that improves structural accuracy by rebuilding side chains and performing molecular dynamics-based energy minimization. This refinement enhances both global and local features of the protein model, ensuring that residue packing and backbone conformations are more physically realistic [37, 38].

2.7 Quality and Error Assessment

To further examine model accuracy, the ProSA-web tool (https://prosa.services.came.sbg.ac.at/prosa.php) was employed. This server calculates a Z-score, which reflects the overall quality of the modeled structure by comparing it to experimentally solved protein structures of similar size. A Z-score within the range of native proteins indicates a reliable model [39]. Finally, the predicted structure was subjected to a quality check using QMEAN (https://swissmodel.expasy.org/qmean), which provides a composite score based on multiple parameters such as local geometry, long-range interactions, and solvation potential. A QMEAN Z-score close to zero confirms that the model aligns well with high-quality experimental structures [40].

2.8 Structural Validation Using SAVES v6.0

To confirm the accuracy of the modeled structure, multiple validation tools were accessed through the SAVES v6.0 server (https://saves.mbi.ucla.edu). This platform combines several independent validation programs, such as PROCHECK, which was used to assess the stereochemical quality of the protein, particularly by analyzing φ and ψ angles in Ramachandran plots. ERRAT evaluated the reliability of non-bonded atomic interactions and detected structural anomalies. Verify 3D examined the compatibility of the 3D model with its amino acid sequence by scoring the environmental profiles of residues. A model with more than 65% of residues scoring above 0.2 is considered structurally acceptable [41, 42].

2.9 Structural Comparison Analysis

To assess the structural deviation between wild-type and mutant PTGER3 proteins, TM-align (https://zhanggroup.org/TM-align) was used. The tool provides the TM-score, indicating global structural similarity (0–1 scale), and RMSD, reflecting the average atomic displacement. A TM-score closer to 1.0 signifies high structural congruence, while a higher RMSD value indicates significant deviation. To evaluate the structural impact of point mutations, the Missense3D tool (http://missense3d.bc.ic.ac.uk) was utilized. It assesses factors such as changes in buried residue exposure, disulfide bond integrity, hydrogen bonding, steric clashes, and alterations in internal cavity volume [34, 43].

2.10 Molecular Docking and Ligand Binding sites

The ligands used for docking analysis were retrieved from PubChem (https://pubchem.ncbi.nlm.nih.gov) and LOTUS (https://lotus.naturalproducts.net). These sources offer a wide range of synthetic and natural compounds with annotated biological activities [44, 45]. The FT Site server (https://ftsite.bu.edu) is used for structure-based protein analysis to identify ligand binding sites and provides data relevant to drug development, protein modification, and protein-protein interactions [46]. The three-dimensional structures of the identified binding sites were visualized using PyMOL (https://pymol.org/2), a widely used molecular graphics system for visualizing protein–ligand complexes [37, 47]. Molecular docking between PTGER3 and the selected ligands was performed using the PyRx 0.9.8 platform (https://pyrx.sourceforge.io). The protein structure was first prepared by removing water molecules and adding polar hydrogens, and ligand structures were energy-minimized using the built-in UFF force field. Both global (blind) and local (site-specific) docking modes were employed to explore potential binding pockets. The best-scoring poses, based on binding affinity (kcal/mol), were exported in PDBQT format for subsequent interaction analysis [48].

2.11 Interaction Profiling of Protein-Ligand

To complement results, detailed visualization and interaction mapping were carried out in BIOVIA Discovery Studio Visualizer

(https://www.3ds.com/products-services/biovia/products/molecular-modeling-simulation/biovia-discovery-studio). The key residues and bond geometries were inspected in 3D, and interaction diagrams were generated to illustrate the spatial arrangement and bond distances. This combined approach provided comprehensive insights into the nature, geometry, and relative strength of ligand–PTGER3 interactions [49].

3. RESULTS

3.1 Screening of SNP IDs

A comprehensive analysis of the human PTGER3 gene was conducted to identify single-nucleotide polymorphisms (SNPs). According to data retrieved from the gnomAD and dbSNP NCBI databases, a total of 27,077 SNPs were associated with this gene. Among these, 17,503 SNPs were found within intronic regions, and 22,341 SNPs were located in the coding regions. Of the coding SNPs, 3,125 were classified as non-synonymous (nsSNPs), which are capable of altering the amino acid sequence of the resulting protein, while 1,636 were identified as synonymous SNPs, which do not affect the amino acid sequence. In addition, 1,024 SNPs were mapped to the 3′ untranslated region (3′ UTR), 166 SNPs were located in the 5′ UTR, and a total of 1,188 SNPs were distributed across the UTR regions. These variants are known to influence gene expression through effects on mRNA stability, localization, or translational regulation. For this study, the PTGER3 gene product with UniProt accession number P43115 was selected for further structural and functional analysis. The gene is situated on chromosome 1 at cytogenetic location 1p31.1 and encodes a protein consisting of 390 amino acids, as presented in **Figure 2A**.

3.2 Consequences of deleterious variants

Using the SNPnexus algorithm, a total of 1,220 amino acid substitutions within the *PTGER3* gene were predicted to be deleterious by the SIFT tool, while 2,159 were classified as tolerated and 479 were marked with low confidence. In parallel, PolyPhen analysis identified 848 variants as probably damaging, 824 as possibly damaging, and 2,109 as benign, as illustrated in **Figure 2B**. Based on the combined outcomes of both tools, 51 SNPs were shortlisted for subsequent structural and functional evaluation. Among the 51 SNPs analyzed in the PTGER3 gene, 26 variants exhibited a SIFT score of 0, indicating they are predicted to be highly deleterious with strong confidence. Additionally, 18 of these SNPs were assigned a PolyPhen-2 score of 1, suggesting they are probably damaging with the highest level of certainty. Notably, 10 SNPs showed both a SIFT score of 0 and a PolyPhen-2 score of 1, highlighting a strong consensus between the two prediction tools regarding their potential pathogenicity. Variants considered neutral or non-deleterious by either tool were excluded from further analysis and the final list of selected SNPs is presented in **Table 1**.

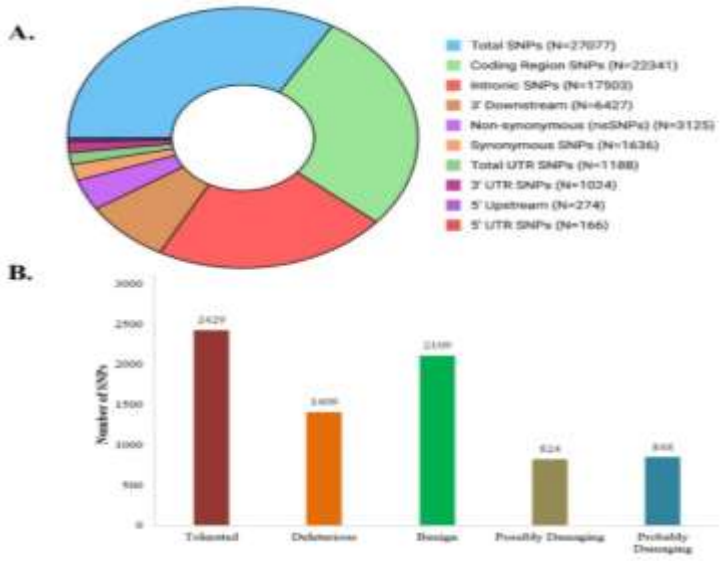


Figure 2. A. Donut representation of SNP distribution in the human PTGER3 gene. **B.** Bar plot illustrating the classification of SNPs predicted by SIFT and PolyPhen tools based on their functional impact.

Furthermore, rs1374103504 (V64G) was uniquely identified as possibly damaging according to PANTHER, while 42 variants were predicted to be probably benign, and R333H, L329S, P162A, M151V, R75C, T277M, C208W, and A235V were classified as probably damaging. According to PredictSNP, 16 nsSNPs, including L354I, N36D, E81Q, V181L, V196M, G213W, L186V, Q359R, K356R, F132I, C325G, G286A, W164R, G93S, T206M, and W25R, were predicted to be neutral, while 35 mutations, such as V113M, R75H, T171R, R119C, T38K, A235V, A189P, S82C, V64G, W25R, S258Y, R75C, V109G, C14R, L239F, C358R, R80W, P162A, M151V, S126L, G93R, V345F, R333H, L329S, C289F, Q283H, E279Q, E279K, T277M, C208W, A189V, W182C, H163Q, and S126W, were classified as deleterious. PolyPhen-2 (HumDiv) predicted 50 SNPs as probably damaging, with only rs756617152 (C14R) identified as benign, as presented in **Table 1**.

Table 1. Functional impact of SNPs by SIFT, PolyPhen, PolyPhen-2, PredictSNP, and PANTHER scores

Rs ID	A.A	SIFT	Score	Polyphen	Score	PolyPhen 2	Score	Predict SNP	PANTHER
rs1408311867	L354I	Deleterious	0	Probably Damaging	0.909	Probably Damaging	1	Neutral	Probably Benign
rs1459721904	V113M	Deleterious	0	Probably Damaging	0.91	Probably Damaging	0.991	Deleterious	Probably Benign
rs1484658630	R75H	Deleterious	0.02	Probably Damaging	0.911	Probably Damaging	0.965	Deleterious	Probably Benign
rs1193790348	N36D	Deleterious	0.02	Probably Damaging	0.912	Probably Damaging	0.979	Neutral	Probably Benign
rs529860827	T171R	Deleterious	0	Probably Damaging	0.914	Probably Damaging	0.999	Deleterious	Probably Benign
rs201372975	E81Q	Deleterious	0.02	Probably Damaging	0.915	Probably Damaging	1	Neutral	Probably Benign
rs778228959	R119C	Deleterious	0.03	Probably Damaging	0.917	Probably Damaging	1	Deleterious	Probably Benign
rs755238098	T38K	Deleterious	0.03	Probably Damaging	0.917	Probably Damaging	0.719	Deleterious	Probably Benign
rs200372986	V181L	Deleterious	0.01	Probably Damaging	0.918	Probably Damaging	0.753	Neutral	Probably Benign
rs748707585	V196M	Deleterious	0.02	Probably Damaging	0.919	Probably Damaging	1	Neutral	Probably Benign
rs140919282	A235V	Deleterious	0	Probably Damaging	0.92	Probably Damaging	0.965	Deleterious	Probably Damaging
rs1460287641	A189P	Deleterious	0	Probably Damaging	0.921	Probably Damaging	1	Deleterious	Probably Benign
rs769768294	S82C	Deleterious	0.01	Probably Damaging	0.927	Probably Damaging	0.997	Deleterious	Probably Benign
rs766690696	G213W	Deleterious	0.02	Probably Damaging	0.928	Probably Damaging	0.999	Neutral	Probably Benign
rs1166049830	L186V	Deleterious	0.04	Probably Damaging	0.929	Probably Damaging	0.938	Neutral	Probably Benign
rs1374103504	V64G	Deleterious	0	Probably Damaging	0.931	Probably Damaging	1	Deleterious	Possibly Damaging
rs1018987601	W25R	Deleterious	0	Probably Damaging	0.931	Probably Damaging	0.996	Deleterious	Probably Benign
rs1047633968	S258Y	Deleterious	0.03	Probably Damaging	0.935	Probably Damaging	0.999	Deleterious	Probably Benign
rs780510896	G226C	Deleterious	0.02	Probably Damaging	0.947	Probably Damaging	1	Neutral	Probably Benign
rs1186877444	R75C	Deleterious	0	Probably Damaging	0.947	Probably Damaging	1	Deleterious	Probably Benign
rs1276026089	V109G	Deleterious	0.03	Probably Damaging	0.95	Probably Damaging	1	Deleterious	Probably Benign

rs756617152	C14R	Deleterious	0	Probably Damaging	0.952	Benign	0.0003	Deleterious	Probably Benign
rs767696491	L239F	Deleterious	0	Probably Damaging	0.954	Probably Damaging	0.999	Neutral	Probably Benign
rs1186877444	R75C	Deleterious	0.01	Probably Damaging	0.954	Probably Damaging	1	Deleterious	Probably Benign
rs1384909748	C358R	Deleterious	0.03	Probably Damaging	0.998	Probably Damaging	1	Deleterious	Probably Benign
rs926117146	R80W	Deleterious	0.02	Probably Damaging	0.998	Probably Damaging	1	Deleterious	Probably Benign
rs976618124	Q359R	Deleterious	0	Probably Damaging	0.999	Probably Damaging	0.988	Neutral	Probably Benign
rs1230642945	K356R	Deleterious	0.03	Probably Damaging	0.999	Probably Damaging	0.998	Neutral	Probably Benign
rs1177109819	P162A	Deleterious	0	Probably Damaging	0.999	Probably Damaging	1	Deleterious	Probably Damaging
rs774251920	M151V	Deleterious	0	Probably Damaging	0.999	Probably Damaging	1	Deleterious	Probably Damaging
rs1461251659	F132I	Deleterious	0	Probably Damaging	0.999	Probably Damaging	1	Neutral	Probably Benign
rs1230757090	S126L	Deleterious	0	Probably Damaging	0.999	Probably Damaging	1	Deleterious	Probably Benign
rs1474081811	G93R	Deleterious	0.01	Probably Damaging	0.999	Probably Damaging	1	Deleterious	Probably Benign
rs1395647928	V345F	Deleterious	0	Probably Damaging	1	Probably Damaging	1	Deleterious	Probably Benign
rs1487698090	R333H	Deleterious	0.01	Probably Damaging	1	Probably Damaging	1	Deleterious	Probably Damaging
rs1480528850	L329S	Deleterious	0	Probably Damaging	1	Probably Damaging	1	Deleterious	Probably Damaging
rs1365332790	C325G	Deleterious	0.02	Probably Damaging	1	Probably Damaging	1	Neutral	Probably Benign
rs1309132187	C289F	Deleterious	0.01	Probably Damaging	1	Probably Damaging	1	Deleterious	Probably Benign
rs757460013	G286A	Deleterious	0	Probably Damaging	1	Probably Damaging	1	Neutral	Probably Benign
rs749093746	Q283H	Deleterious	0	Probably Damaging	1	Probably Damaging	1	Deleterious	Probably Benign
rs748106085	E279Q	Deleterious	0	Probably Damaging	1	Probably Damaging	1	Deleterious	Probably Benign
rs748106085	E279K	Deleterious	0	Probably Damaging	1	Probably Damaging	1	Deleterious	Probably Benign
rs1377942199	T277M	Deleterious	0	Probably Damaging	1	Probably Damaging	1	Deleterious	Probably Benign
rs758267186	C208W	Deleterious	0	Probably Damaging	1	Probably Damaging	1	Deleterious	Probably Damaging
rs1340918654	T206M	Deleterious	0.03	Probably Damaging	1	Probably Damaging	1	Deleterious	Probably Benign
rs1320861099	A189V	Deleterious	0	Probably Damaging	1	Probably Damaging	1	Deleterious	Probably Benign
rs759776269	W182C	Deleterious	0.02	Probably Damaging	1	Probably Damaging	1	Deleterious	Probably Benign
rs747455158	W164R	Deleterious	0	Probably Damaging	1	Probably Damaging	1	Neutral	Probably Benign
rs562873836	H163Q	Deleterious	0.03	Probably Damaging	1	Probably Damaging	1	Deleterious	Probably Benign
rs1230757090	S126W	Deleterious	0.01	Probably Damaging	1	Probably Damaging	1	Deleterious	Probably Benign
rs1474081811	G93S	Deleterious	0	Probably Damaging	1	Probably Damaging	1	Neutral	Probably Benign

3.3 Functional and Stability Analysis of SNPs

A comprehensive evaluation of 51 SNPs was conducted using five predictive tools SNP & GO, SuSPect, Meta-SNP, MUpro, and i-Stable. Among these, SNP&GO identified R119C, W25R, C14R, C358R, M151V, V345F, R333H, L329S, C325G, and E279Q as disease-associated variants, while the remaining mutations were predicted to be neutral. The SuSPect scores highlighted A189P, M151V, R333H, and C208W as potentially damaging due to their high pathogenicity scores, such as M151V with a score of 61 and R333H with a score of 43. Meta-SNP classified 32 mutations, including R75H, G93R, V64G, A189P, L329S, and R333H, as disease-related, further supporting their potential harmful effects on protein function. The MUpro results indicated that V109G, L329S, V345F, and G93R led to decreased protein stability, whereas S126L, R75C, and A189V were predicted to increase stability. Similarly, i-Stable predictions revealed that mutations such as A189P, S82C, R75C, C325G, and S126W contributed to increased stability, while most others caused destabilization. Moreover, L329S, R333H, M151V, G93R, and V345F consistently appeared deleterious across multiple tools, suggesting a significant potential to disrupt protein function and contribute to disease mechanisms, as given in **Table 2**.

Table 2. Disease association and protein stability predictions for PTGER3 SNPs

rsIDs	A.A	SNP&GO	Score	Suspect	Pred	Meta SNP	Mu Pro	Conf. Score	i-Stable	Conf. Score
rs1408311867	L354I	Neutral	8	25	Disease	Neutral	Decrease	-0.848356	Decrease	0.847616
rs1459721904	V113M	Neutral	8	17	Neutral	Neutral	Decrease	-0.993693	Decrease	0.84768
rs1484658630	R75H	Neutral	7	28	Disease	Neutral	Decrease	-1.019169	Increase	0.756269
rs1193790348	N36D	Neutral	8	30	Disease	Neutral	Decrease	-0.889008	Increase	0.63378
rs529860827	T171R	Neutral	2	7	Neutral	Neutral	Decrease	-0.898355	Decrease	0.782252
rs201372975	E81Q	Neutral	9	8	Neutral	Neutral	Decrease	-0.856019	Decrease	0.809628
rs778228959	R119C	Disease	0	24	Disease	Disease	Decrease	-0.81567	Decrease	0.788634
rs755238098	T38K	Neutral	7	19	Neutral	Neutral	Decrease	-1.018213	Decrease	0.755893
rs200372986	V181L	Neutral	6	30	Disease	Neutral	Decrease	-1.007592	Decrease	0.83232
rs748707585	V196M	Neutral	6	19	Neutral	Neutral	Decrease	-0.85634	Decrease	0.798455
rs140919282	A235V	Neutral	6	9	Neutral	Disease	Decrease	-0.826645	Increase	0.786669
rs1460287641	A189P	Neutral	1	62	Disease	Disease	Decrease	-1.572669	Increase	0.537228
rs769768294	S82C	Neutral	9	19	Neutral	Neutral	Decrease	-0.930775	Increase	0.806544
rs766690696	G213W	Neutral	4	6	Neutral	Neutral	Decrease	-1.247769	Decrease	0.540413
rs1166049830	L186V	Neutral	9	25	Disease	Disease	Decrease	-0.615482	Decrease	0.852652
rs1374103504	V64G	Neutral	2	31	Disease	Disease	Decrease	-1.696255	Decrease	0.785928
rs1018987601	W25R	Disease	0	27	Disease	Disease	Decrease	-0.290374	Decrease	0.690121
rs1047633968	S258Y	Neutral	3	14	Neutral	Neutral	Decrease	-0.281069	Increase	0.735238
rs780510896	G226C	Neutral	3	18	Neutral	Disease	Decrease	-0.678604	Increase	0.571979

rs1186877444	R75C	Neutral	2	27	Disease	Neutral	Decrease	-0.503819	Increase	0.786034
rs1276026089	V109G	Neutral	4	49	Disease	Disease	Decrease	-1.718389	Decrease	0.876152
rs756617152	C14R	Disease	3	24	Disease	Disease	Decrease	-0.780976	Increase	0.666098
rs767696491	L239F	Neutral	8	19	Neutral	Disease	Decrease	-0.936674	Decrease	0.693143
rs1186877444	R75C	Neutral	2	27	Disease	Disease	Decrease	-0.878761	Increase	0.786034
rs1384909748	C358R	Disease	4	24	Disease	Disease	Decrease	-0.556876	Decrease	0.663485
rs926117146	R80W	Neutral	3	66	Disease	Disease	Decrease	-0.490726	Decrease	0.755208
rs976618124	Q359R	Neutral	6	6	Neutral	Neutral	Decrease	-0.628473	Decrease	0.66428
rs1230642945	K356R	Neutral	9	11	Neutral	Neutral	Decrease	-1.676727	Increase	0.799426
rs1177109819	P162A	Neutral	4	68	Disease	Disease	Decrease	-1.194018	Decrease	0.650331
rs774251920	M151V	Disease	1	61	Disease	Disease	Decrease	-0.970062	Decrease	0.77673
rs1461251659	F132I	Neutral	2	20	Neutral	Neutral	Decrease	0.146394	Decrease	0.638367
rs1230757090	S126L	Neutral	3	22	Disease	Disease	Increase	-1.019426	Increase	0.5
rs1474081811	G93R	Neutral	1	25	Disease	Disease	Decrease	-1.11659	Increase	0.600356
rs1395647928	V345F	Disease	1	60	Disease	Disease	Decrease	-0.796009	Decrease	0.878089
rs1487698090	R333H	Disease	1	43	Disease	Disease	Decrease	-1.796958	Decrease	0.813934
rs1480528850	L329S	Disease	0	31	Disease	Disease	Decrease	-2.366246	Decrease	0.888246
rs1365332790	C325G	Disease	1	12	Neutral	Disease	Decrease	-0.529422	Decrease	0.86121
rs1309132187	C289F	Disease	3	16	Neutral	Disease	Decrease	-0.653078	Increase	0.537941
rs757460013	G286A	Neutral	8	6	Neutral	Neutral	Decrease	-1.001361	Decrease	0.800562
rs749093746	Q283H	Neutral	0	25	Disease	Disease	Decrease	-0.606706	Decrease	0.846859
rs748106085	E279Q	Disease	0	15	Neutral	Neutral	Decrease	-0.876281	Decrease	0.624845
rs748106085	E279K	Neutral	2	6	Neutral	Disease	Decrease	-0.17976	Decrease	0.585286
rs1377942199	T277M	Neutral	4	24	Disease	Neutral	Decrease	-0.981825	Increase	0.80312
rs758267186	C208W	Disease	3	53	Disease	Disease	Decrease	-0.420669	Decrease	0.514518
rs1340918654	T206M	Neutral	2	26	Disease	Disease	Decrease	-0.532459	Decrease	0.635878
rs1320861099	A189V	Neutral	4	43	Disease	Disease	Decrease	-0.560929	Increase	0.79385
rs759776269	W182C	Neutral	1	76	Disease	Disease	Decrease	-0.891777	Increase	0.626829
rs747455158	W164R	Disease	2	10	Neutral	Disease	Decrease	-0.247905	Decrease	0.82578
rs562873836	H163Q	Neutral	2	43	Disease	Disease	Decrease	-0.406036	Decrease	0.805946

rs1230757090	S126W	Neutral	1	28	Disease	Disease	Decrease	-1.21953	Increase	0.73012
rs1474081811	G93S	Neutral	7	16	Neutral	Neutral	Decrease	-0.848356	Decrease	0.845494

3.5 Effect of Mutations on Protein Structure

The structural impact of 51 SNPs in the PTGER3 gene was assessed using the HOPE server as given in **Table 3**. The analysis indicated that 30 mutations including V113M, T171R, A189P, G213W, A235V, L239F, S258Y, G226C, K356R, L329S, R333H, M151V, F132I, S126L, V345F, Q283H, E279K, T277M, C208W, T206M, A189V, G286A, C289F, C325G, L354I, and resulted in amino acid substitutions that were larger than the wild-type residues, potentially causing steric hindrance or conformational strain in the protein structure. In contrast, 19 mutations, including R75H, N36D, S82C, L186V, V64G, W25R, R75C, F132I, W182C, G93R, G93S, C325G, L354I, R333H, and V345F, involved smaller residues, potentially reducing side chain interactions and local structural stability. Two variants, E81Q and E279Q, resulted in residues of similar size, implying minimal size-driven effects.

Regarding residue environment, 14 mutations increased local hydrophobicity, which may affect protein folding or membrane association. Thirteen mutations occurred at moderately conserved regions while 24 mutations were located at highly conserved residues, suggesting critical roles in structural integrity or functional domains. In functional effect, the HOPE server classified 22 mutations as possibly damaging, 18 mutations as probably damaging, and 11 mutations as deleterious. These observations suggest that the 15 SNPs may significantly alter the structural and functional dynamics of the PTGER3 receptor, potentially affecting its role in prostaglandin signaling and are used for further analysis. These substitutions of the wild-type amino acid with a larger mutant residue, which may introduce steric hindrance, and a predicted effect of "probably damaging" on the protein's structure or function

Table 3. Structural impact of PTGER3 mutations predicted by the HOPE server

rsID	Variant	Mutant Size	SNP Location	Effect of Polymorphism
rs1408311867	L354I	Smaller	More hydrophobic	Possibly Damaging
rs1459721904	V113M	Bigger	Conserved	Possibly Damaging
rs1484658630	R75H	Smaller	Conserved	Probably Damaging
rs1193790348	N36D	Smaller	More hydrophobic	Possibly Damaging
rs529860827	T171R	Bigger	Conserved	Probably Damaging
rs201372975	E81Q	Similar	Conserved	Possibly Damaging
rs778228959	R119C	Smaller	More hydrophobic	Damaging
rs755238098	T38K	Bigger	More hydrophobic	Probably Damaging
rs200372986	V181L	Bigger	More hydrophobic	Possibly Damaging
rs748707585	V196M	Bigger	Conserved	Possibly Damaging
rs140919282	A235V	Bigger	Conserved	Possibly Damaging
rs1460287641	A189P	Bigger	Conserved	Probably Damaging
rs769768294	S82C	Smaller	More hydrophobic	Damaging
rs766690696	G213W	Bigger	More hydrophobic	Probably Damaging
rs1166049830	L186V	Smaller	Conserved	Possibly Damaging
rs1374103504	V64G	Smaller	More hydrophobic	Possibly Damaging
rs1018987601	W25R	Smaller	More hydrophobic	Damaging
rs1047633968	S258Y	Bigger	More hydrophobic	Probably Damaging

rs780510896	G226C	Bigger	Conserved	Probably Damaging
rs1276026089	V109G	Smaller	More hydrophobic	Possibly Damaging
rs756617152	C14R	Bigger	Conserved	Damaging
rs767696491	L239F	Bigger	More hydrophobic	Possibly Damaging
rs1186877444	R75C	Smaller	Conserved	Probably Damaging
rs1384909748	C358R	Bigger	Highly Conserved	Damaging
rs926117146	R80W	Bigger	More hydrophobic	Probably Damaging
rs976618124	Q359R	Bigger	Highly Conserved	Damaging
rs1230642945	K356R	Bigger	Highly Conserved	Damaging
rs1177109819	P162A	Smaller	Highly Conserved	Possibly Damaging
rs774251920	M151V	Smaller	Highly Conserved	Possibly Damaging
rs1461251659	F132I	Smaller	Highly Conserved	Possibly Damaging
rs1230757090	S126L	Bigger	Highly Conserved	Possibly Damaging
rs1474081811	G93R	Bigger	Highly Conserved	Probably Damaging
rs1395647928	V345F	Bigger	Highly Conserved	Possibly Damaging
rs1487698090	R333H	Smaller	Highly Conserved	Probably Damaging
rs1480528850	L329S	Smaller	Highly Conserved	Possibly Damaging
rs1365332790	C325G	Smaller	Highly Conserved	Damaging
rs1309132187	C289F	Bigger	Highly Conserved	Possibly Damaging
rs757460013	G286A	Bigger	Highly Conserved	Possibly Damaging
rs749093746	Q283H	Bigger	Highly Conserved	Probably Damaging
rs748106085	E279Q	Similar	Highly Conserved	Possibly Damaging
rs748106085	E279K	Bigger	Highly Conserved	Probably Damaging
rs1377942199	T277M	Bigger	Highly Conserved	Probably Damaging
rs758267186	C208W	Bigger	Highly Conserved	Damaging
rs1340918654	T206M	Bigger	Highly Conserved	Probably Damaging
rs1320861099	A189V	Bigger	Highly Conserved	Probably Damaging
rs759776269	W182C	Smaller	Conserved	Damaging
rs747455158	W164R	Smaller	Highly Conserved	Probably Damaging
rs562873836	H163Q	Smaller	Highly Conserved	Possibly Damaging
rs1230757090	S126W	Bigger	More hydrophobic	Probably Damaging
rs1474081811	G93S	Bigger	Conserved	Possibly Damaging

3.6 PTGER3 protein modeling and validation

The three-dimensional structure of the human PTGER3 receptor was modelled to evaluate the impact of 15 highly conserved, probably damaging variants. The full-length sequence (UniProt P43115, 1–390 aa) was aligned to 50 template structures showing 100% sequence identity; the AlphaFold DB entry PE2R3_HUMAN (PDB chain P43115 A) was selected as the primary template. Initial modelling was performed in PyMOL, followed by refinement with GalaxyRefine. Among the five Galaxy-generated models, model 05 displayed the best stereochemistry and was chosen for further analysis, as shown in **Figure 3A**.

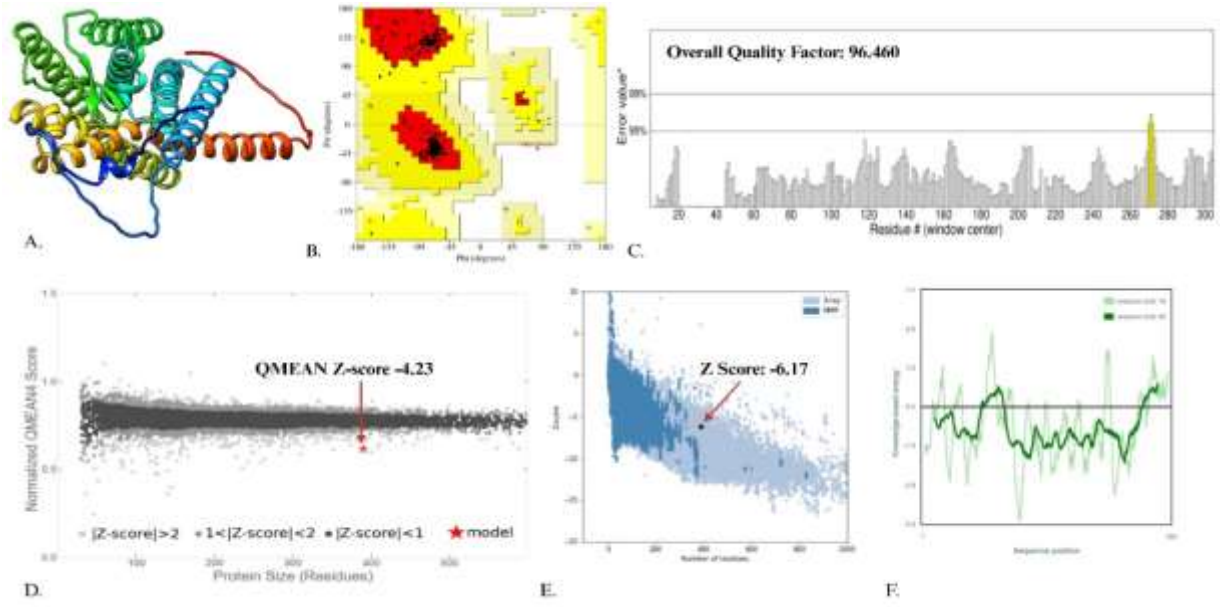


Figure 3. Structural Modeling and Quality Assessment of PTGER3 Protein A) Three-dimensional model of PTGER3 **B)** Ramachandran plot analysis **C)** ERRAT quality factor **D)** QMEAN Z-score profile **E)** ProSA Z-score analysis **F)** Local model quality assessment.

The stereochemical integrity of the refined PTGER3 protein structure was evaluated through Ramachandran plot analysis, which showed that 98.0% of the residues are located in core (favored) regions, 2.0% in allowed regions, and none in generously allowed or disallowed regions **(Figure 3B)**. This distribution reflects a structurally complete model with a reliable backbone conformation. Additionally, the ERRAT analysis produced an Overall Quality Factor of 96.4602, confirming the model's high structural accuracy **Figure 3C**. The model QMEAN Z-score of −4.23 **(Figure 3D)** and ProSA Z-score of −6.17 **(Figure 3E)** and energy plot **(Figure 3F)**, although indicating some moderate instability, fall within acceptable limits for G protein-coupled receptor (GPCR) models of similar size and complexity. Collectively, the validation parameters confirm that the refined PTGER3 protein model possesses the structural integrity required for advanced functional and structural analysis. By Missense 3D, C358R and E279K were predicted to significantly expand internal cavity volume, while T277M disrupted a buried hydrogen bond, indicating potential core destabilization **(Figure 4)**. These three variants were therefore selected for subsequent molecular docking studies as presented in **Table 4**. In contrast, the other assessed substitutions showed no major structural disturbances, suggesting that their effects may arise from more refined conformational shifts or modifications of local interaction networks.

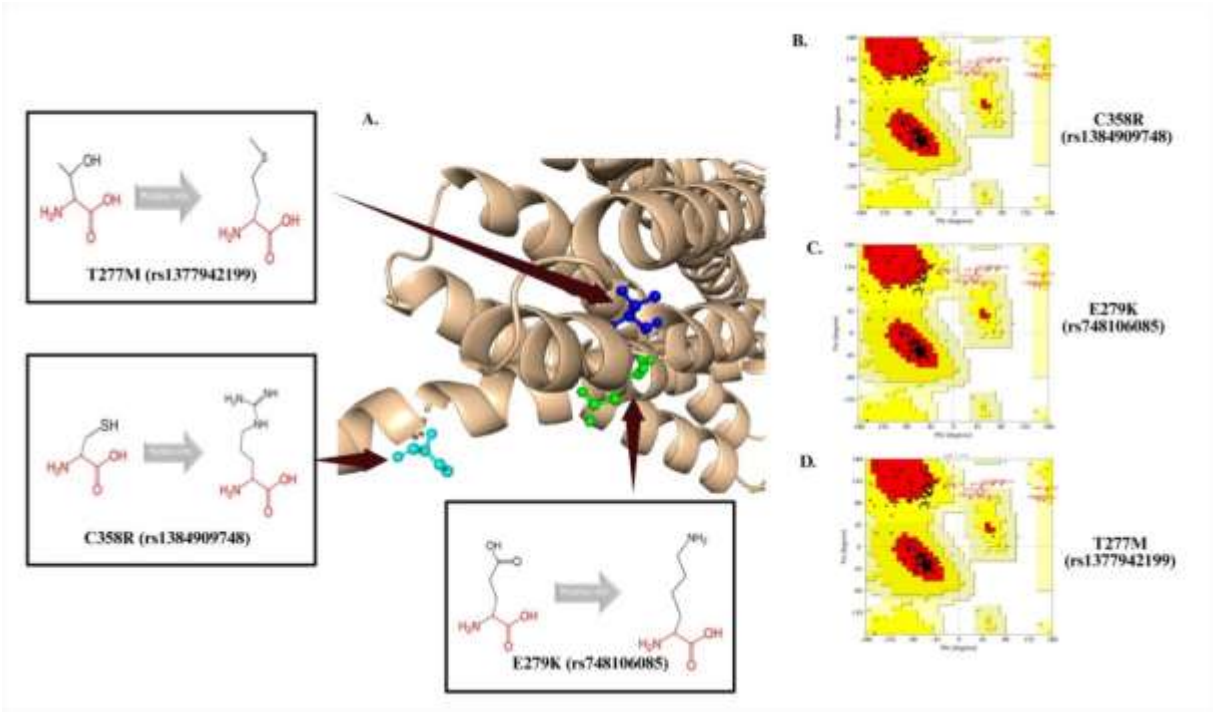


Figure 4. A. Cartoon representation of PTGER3 variants **B.** Ramachandran plot of C358R (rs1384909748) **C.** Ramachandran plot of E279K (rs748106085) **D.** Ramachandran plot of T277M (rs1377942199).

Table 4. Comprehensive validation and structural analysis of 15 prioritized PTGER3 variants using SAVES v6.1, TM-score, and Missense3D structural impact predictions

Variant	ERRAT	Core (%)	Allowed (%)	Generous (%)	Disallowed (%)	Verify3D (%)	RMSD	TM-score	Missense3D Effect
A189V	94.1349	97.70	2.00	0.00	0.30	29.23	0.41	0.99678	No effect
C358R	97.9042	98.00	1.70	0.00	0.30	29.23	0.35	0.99763	Cavity altered (93.744 Å³)
E279K	98.2196	97.70	2.00	0.00	0.30	32.56	0.39	0.99717	Cavity altered (72.792 Å³)
G226C	97.9472	98.00	1.70	0.30	0.00	34.87	0.41	0.99689	No effect
G93R	95.3216	97.10	2.60	0.00	0.30	31.03	0.24	0.99887	No effect
R333H	96.7262	97.40	2.60	0.00	0.00	40.77	0.41	0.99677	No effect
R80W	92.9204	96.80	2.90	0.00	0.30	28.72	0.25	0.99882	No effect
S126W	92.5816	97.10	2.60	0.30	0.00	34.36	0.24	0.99887	No effect
S258Y	94.0476	96.60	3.20	0.00	0.30	36.41	0.26	0.99870	No effect
T171R	93.1953	97.10	2.60	0.00	0.30	33.08	0.24	0.99890	No effect
T206M	95.5490	97.40	2.30	0.00	0.30	27.69	0.29	0.99846	No effect

T277M	97.0414	97.40	2.30	0.30	0.00	31.54	0.39	0.99710	Buried H-bond breakage
T38K	95.0147	97.40	2.00	0.30	0.30	29.49	0.29	0.99845	No effect
V113M	92.8994	97.40	2.30	0.30	0.00	30.00	0.28	0.99849	No effect
W164R	94.1520	97.70	2.00	0.00	0.30	32.31	0.23	0.99898	No effect

3.7 Virtual Screening and FT sites prediction

Form PubChem and LOTUS databases, 12 ligands were selected based on their known pharmacological profiles and their potential to modulate PTGER3-mediated inflammatory responses in conjunctivitis. Each of these compounds offers unique therapeutic benefits that could help alleviate ocular inflammation by targeting the EP3 receptor pathway. Eugenol inhibits the synthesis of prostaglandin E_2 by targeting cyclooxygenase enzymes, thereby potentially reducing PTGER3 activation. Proflavine exhibits strong antimicrobial activity, which may indirectly suppress inflammation caused by bacterial infections of the conjunctiva. Benzamidine and pepstatin A act as protease inhibitors and could play a protective role by preventing tissue degradation and maintaining receptor structure in inflamed ocular tissues. Plant-derived compounds such as cinnamal and galegine are recognized for their antioxidant and anti-inflammatory properties, which may help to minimize oxidative stress and cytokine production, reducing the risk of excessive EP3 receptor stimulation [50, 51]. Furthermore, methylcytosine holds potential for regulating local inflammation through epigenetic modulation. Glutathione and γ-mangostin, both strong antioxidants, may protect ocular cells from reactive oxygen species (ROS), stabilize the receptor conformation, and enhance the fidelity of ligand binding. Isobutylbenzene, a structural analogue of nonsteroidal anti-inflammatory drugs, presents a promising lead compound for developing EP3 antagonists. In viral conjunctivitis, 8-iodoguanine could help suppress viral replication, while galactonolactone may influence immune signaling by modulating glycosylation patterns involved in receptor interactions. Phenylthiourea helps limit oxidative epithelial damage, potentially reducing stress induced by receptor-targeted therapies. Ganomycin-I, known for its broad-spectrum antimicrobial effects, may reduce bacterial colonization and associated inflammatory triggers that activate EP3 signaling. Overall, these ligands demonstrate a broad spectrum of anti-inflammatory and anti-infective mechanisms, making them valuable candidates for further optimization as PTGER3-targeted therapeutics in conjunctivitis and related ocular disorders [52].

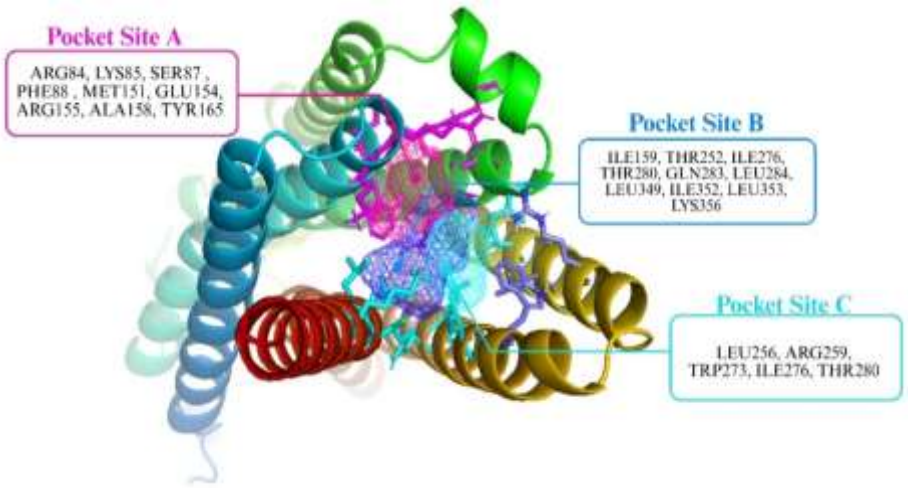


Figure 5. Predicted ligand-binding sites of the PTGER3 protein, as identified by FTsite.

Binding site prediction analysis using the FTsite server revealed three distinct ligand-binding pockets on the PTGER3 protein, labeled as Sites A, B, and C (**Figure 5**). Site A comprises residues ARG84, LYS85, SER87, PHE88, MET151, GLU154, ARG155, ALA158, and TYR165. This region is located in the upper portion of the receptor and is rich in polar and charged residues, indicating its potential to form hydrogen bonds and electrostatic interactions with ligands. Site B is positioned more centrally and includes residues ILE159, THR252, ILE276, THR280, GLN283, LEU284, LEU349, ILE352, LEU353, and LYS356. The combination of hydrophobic and polar amino acids in this pocket suggests it may support both hydrophobic and hydrogen bonding interactions. Site C is composed of LEU256, ARG259, TRP273, ILE276, and THR280, forming a smaller binding pocket slightly below Site B. The arrangement of hydrophobic and charged residues in this region indicates a potential role in secondary ligand stabilization.

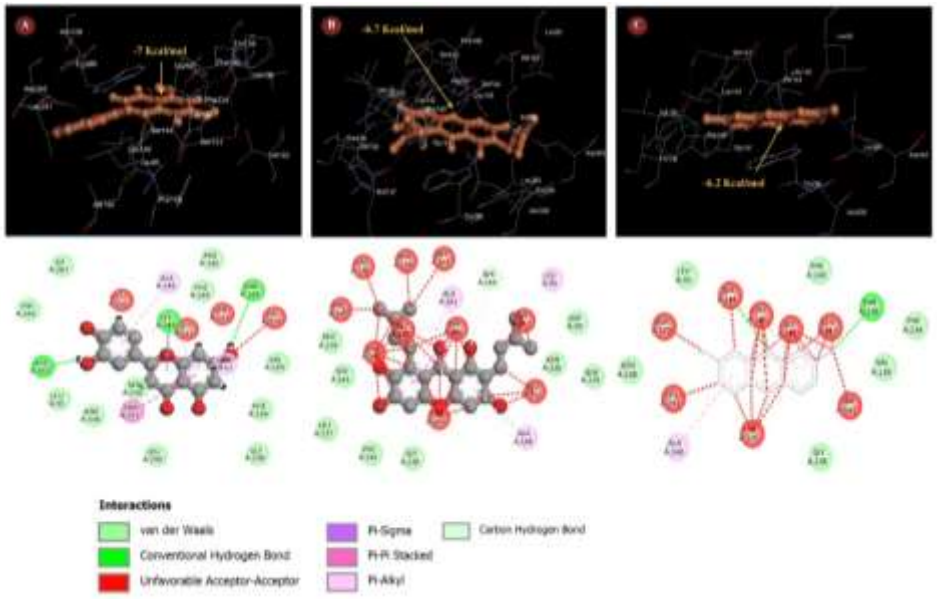


Figure 6. Protein–Ligand Docking Interactions of Wild-Type with (A) Luteolin, (B) G-Mangostin, and (C) Proflavine.

Docking studies were performed to evaluate the binding affinity and interaction patterns of selected ligands within these predicted pockets of PTGER3 protein (**Table 5**). Luteolin displayed a strong binding affinity of −7.0 kcal/mol and formed several key interactions with wild type protein (PTGER3), including hydrogen bonds with ASP342, THR138, and SER144. It also established π-alkyl and π–π stacking interactions with residues such as TRP295 and ALA148, with van der Waals contacts involving ASN338, ILE287, and PHE140. Some unfavorable acceptor–acceptor interactions were noted with VAL139 and LEU142 (**Figure 6A**). γ-Mangostin, with a binding energy of −6.7 kcal/mol, formed a hydrogen bond with SER144 and π-alkyl interactions with TRP295 and ALA148, but also displayed several unfavorable donor–donor interactions with LEU145, GLY141, and SER143. Additionally, it engaged in van der Waals interactions with PHE146, GLY238, and LEU237 (**Figure 6B**). Proflavine showed a binding energy of −6.2 kcal/mol and interacted through a hydrogen bond with THR138 and π-alkyl interactions with ALA148, though it also presented unfavorable donor–donor interactions with TRP295, LEU145, SER144, and GLY141. Van der Waals interactions were observed with PHE140, GLY238, and LEU95 (**Figure 6C**). Importantly, several of the residues involved in ligand interactions such as ALA148, LEU145, ILE287, THR138, and LEU299 were also identified as part of the FTsite-predicted binding

pockets, confirming their significance in ligand stabilization. These findings highlight the importance of these sites in mediating protein-ligand interactions and support their relevance as targets for the development of selective small-molecule modulators of PTGER3 in ocular inflammatory conditions.

Table 5. Molecular Interactions and Key Binding Residues of Luteolin, G-Mangostin, and Proflavine with Wild-Type PTGER3 Protein

Ligand	Interaction Type	Color/Style	Residues Involved (FT Site residues in bold)
Wild type + Luteolin	Van der Waals	Light green fill	**ILE A:287**, **TYR A:346**, **LEU A:95**, **ASN A:338**, PHE A:140, PHE A:146, PHE A:234, **LEU A:299**, **VAL A:185**, **GLY A:238**
	Conventional Hydrogen Bond	Bright green dashed lines	**ASP A:342**, **THR A:138**
	Unfavorable Bump	Red fill + red dashed lines	**VAL A:139**, **SER A:143**, **GLY A:141**, **LEU A:142**, **LEU A:291**
	Pi–Pi Stacked	Pink fill	TRP A:295
	Pi-Alkyl	Light pink fill	**ALA A:148**, **LEU A:145**
Wild type + G-Mangostin	Van der Waals	Light green fill	**SER A:143**, **SER A:144**, PHE A:146, **LEU A:237**, **GLY A:238**, PHE A:234, **GLN A:339**, **ASP A:99**, **ASN A:338**
	Unfavorable Bump	Red fill + red dashed lines	**VAL A:139**, **THR A:138**, **MET A:137**, PHE A:140, **GLY A:141**, **LEU A:142**, **LEU A:145**, **LEU A:291**, **ASP A:342**
	Carbon Hydrogen Bond	Pale green dashed line	**SER A:144**
	Pi–Pi T-shaped	Bright pink dashed lines	TRP A:295
	Pi-Alkyl	Light pink fill	**ALA A:148**, **ALA A:241**, **LEU A:95**
Wild type + Proflavine	Van der Waals	Light green fill	**LEU A:95**, **ASN A:338**, PHE A:140, **VAL A:139**, PHE A:234, **GLY A:238**
	Conventional Hydrogen Bond	Bright green dashed lines	**THR A:138**
	Unfavorable Bump	Red fill + red dashed lines	**ASP A:342**, **SER A:144**, **LEU A:145**, **GLY A:141**, **LEU A:142**, **SER A:143**, **LEU A:291**, TRP A:295
	Pi-Alkyl	Light pink fill	**ALA A:148**

Furthermore, Ganomycin-I, Luteolin, and γ-Mangostin exhibit diverse molecular interactions with the C258R mutant of the PTGER3 protein, as illustrated in **Figure 7**. Ganomycin-I primarily engages the mutant receptor through van der Waals forces involving residues such as PHE146, ILE147, and ASN338 (**Figure 7A**). However, steric clashes are suggested by unfavorable bump interactions with residues like ASP342, SER143, and LEU142. Alkyl interactions with ALA148 and additional pi-alkyl contacts further stabilize its binding, although these are not fully labeled beyond ALA148. Luteolin shows a more complex interaction network, forming van der Waals contacts with LEU95, ASN338, PHE234, GLY238, and LEU299, alongside conventional hydrogen bonds with THR138 (**Figure 7B**). Despite the presence of unfavorable bumps at ASP342, LEU291, SER143, LEU145, and TRP295, luteolin also forms alkyl and pi-alkyl interactions with ALA148, PHE146, and LEU145. Additionally, pi-sigma and pi–pi stacked interactions involving LEU145, PHE140, and PHE146 enhance ligand stabilization. γ-Mangostin demonstrates extensive van der Waals interactions with multiple residues including VAL185, SER144, PHE146, GLY238, and ASN338 (**Figure 7C**). Unfavorable bumps with residues such as THR138, VAL139, MET137, and TRP295 are noted, alongside a carbon hydrogen bond involving SER144. Aromatic interactions like pi–pi T-shaped and pi-alkyl contacts with PHE140, ALA148, LEU95, and LEU145 contribute significantly to its binding affinity. These findings underscore that hydrophobic and van der Waals forces, combined with selective hydrogen bonding and aromatic interactions, play pivotal roles in ligand engagement with the C258R mutant (**Table 6**).

Similarly, in the E279K mutant with G-Mangostin (**Figure 7D**) achieves the highest docking score, forming van der Waals interactions with residues including SER143, SER144, PHE146, LEU237, ASP99, ASN338, and GLN339. Despite unfavorable bump contacts with PHE140, VAL139, and LEU291, it forms a carbon hydrogen bond and pi–pi T-shaped interactions with TRP295, and pi-alkyl interactions

with LEU95, ALA148, and ALA241. Luteolin interacts extensively via van der Waals forces with PHE140, PHE146, LEU95, ASN338, while establishing conventional hydrogen bonds with ASP342, SER143, and LEU145 (**Figure 7E**). Unfavorable acceptor–acceptor interactions with VAL139, LEU142, and GLY141 were observed. Additional pi-sigma, pi–pi stacked, and pi-alkyl interactions further support ligand binding. Ganomycin-I binds through van der Waals interactions with VAL290, ASN338, PHE140, and other residues but shows unfavorable bump interactions at SER143, SER144, and LEU145 (**Figure 7F**). Pi-alkyl interactions with ALA148 suggest hydrophobic stabilization, indicating that the E279K mutation maintains critical ligand-binding capacity (**Table 6**).

In the T277M mutant, γ-Mangostin maintains multiple van der Waals contacts similar to other mutants, involving SER143, SER144, PHE146, GLY238 along with unfavorable bumps and hydrogen bonding to TRP295. Pi–pi T-shaped and pi-alkyl interactions also contribute to ligand affinity (**Figure 7G**). Luteolin exhibits van der Waals interactions with ILE287, TYR346, and LEU95, conventional hydrogen bonds with ASP342, SER144, LEU145, and THR138, and aromatic pi-sigma and pi–pi stacked interactions (**Figure 7H**). Proflavine interacts via van der Waals forces with LEU95, ASN338, PHE140, and others, forms a hydrogen bond with THR138 (**Figure 7I**), but also displays several unfavorable bumps and acceptor–acceptor interactions. Pi-alkyl interactions with ALA148 further stabilize the ligand (**Table 6**).

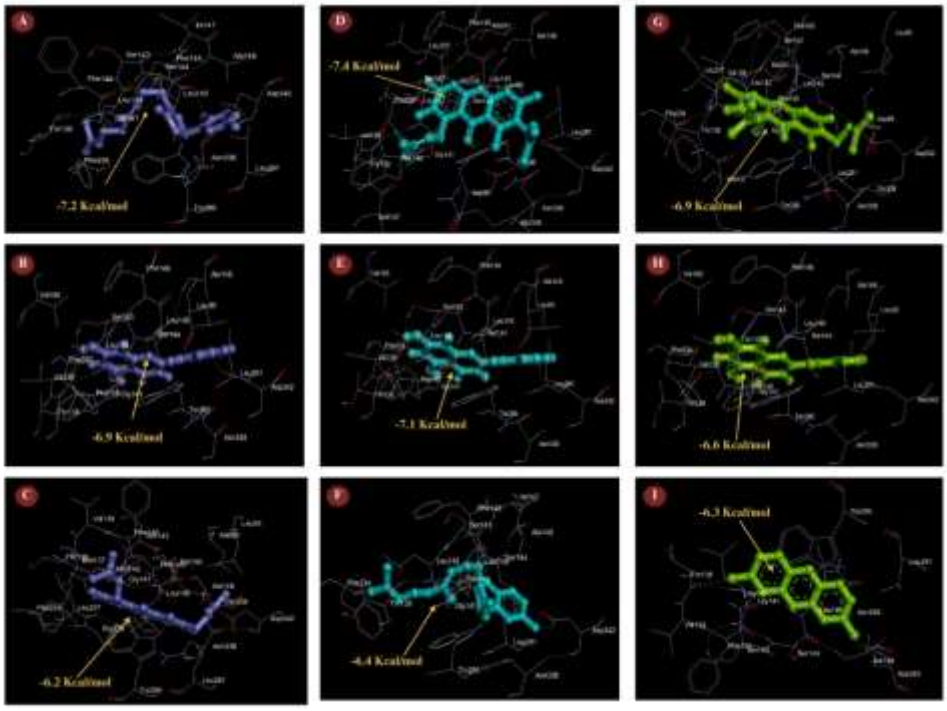


Figure 7. Molecular docking interactions of T277M, E279K, and C348R with G-Mangostin, Ganomycin-I, Luteolin, and Proflavine. The image displays interacting residues, types of bonds, and binding energies (kcal/mol) as visualized using Discovery Studio Biovia.

These interaction profiles highlight that despite mutations, critical residues within the PTGER3 binding pocket continue to participate in ligand stabilization through a combination of hydrophobic forces, hydrogen bonding, and aromatic stacking. Such resilience suggests potential for these compounds to act as effective modulators of mutated PTGER3 in conjunctivitis. Given PTGER3 role in

mediating inflammatory responses in the conjunctiva, targeting these mutant forms could offer therapeutic benefit in managing conjunctival inflammation associated with infection or allergic stimuli. However, the presence of unfavorable steric clashes and altered residue environments caused by mutations may affect ligand binding affinities and selectivity, posing challenges for drug design. Future studies should focus on optimizing these scaffolds to improve binding specificity and reduce steric hindrance. Experimental validation of these in silico findings will be crucial to translating these insights into clinically relevant conjunctivitis therapies.

Table 6. Interaction profiles of G-mangostin, luteolin, proflavine, and ganomycin-I with T277M, E279K, C348R mutants as visualized using Discovery Studio Biovia.

Ligand + Mutant	Interaction Type	Color/Style	Residues Involved
C348R + Ganomycin-I	Van der Waals	Light green fill	PHE A:146, ILE A:147, ASN A:338
	Unfavorable Bump	Red fill + red dashed lines	ASP A:342, SER A:143, LEU A:142
	Alkyl	Light pink fill	**ALA A:148**
	Pi-Alkyl	Purple-pink fill	**ALA A:148**
C348R + Luteolin	Van der Waals	Light green fill	LEU A:95, ASN A:338, PHE A:234, GLY A:238, LEU A:299
	Unfavorable Bump	Red fill + red dashed lines	ASP A:342, LEU A:291, SER A:143, LEU A:145, TRP A:295
	Conventional Hydrogen Bond	Green dashed lines	THR A:138
	Alkyl	Light pink fill	**ALA A:148**
	Pi-Alkyl	Light purple/grayish fill	PHE A:146, LEU A:145
	Pi-Sigma	Bright purple lines	LEU A:145
	Pi–Pi Stacked	Pink lines	PHE A:140, PHE A:146
C348R + G-Mangostin	Van der Waals	Light green fill	VAL A:185, SER A:144, PHE A:146, GLY A:238, LEU A:237, PHE A:234, SER A:143, LEU A:242, ASP A:99, ASN A:338, **GLN A:339**
	Unfavorable Bump	Red fill + red dashed lines	THR A:138, VAL A:139, MET A:137, PHE A:140, GLY A:141, LEU A:142, TRP A:295, LEU A:145, LEU A:291, ASP A:342
	Carbon Hydrogen Bond	Thin green dashed line	SER A:144
	Pi–Pi T-shaped	Pink fill	PHE A:140
	Pi-Alkyl	Light purple fill	**ALA A:148**, LEU A:95, LEU A:145
E279K + G-Mangostin	Van der Waals	Light green fill	SER A:143, SER A:144, PHE A:146, LEU A:237, ASP A:99, ASN A:338, **GLN A:339**, GLY A:238, PHE A:234
	Unfavorable Bump	Red fill + red dashed lines	PHE A:140, VAL A:139, THR A:138, MET A:137, GLY A:141, LEU A:142, LEU A:145, ASP A:342, LEU A:291
	Carbon Hydrogen Bond	Gray line	TRP A:295
	Pi–Pi T-shaped	Bright pink dashed lines	TRP A:295
	Pi-Alkyl	Purple-pink fill	LEU A:95, **ALA A:148**, ALA A:241
E279K + Luteolin	Van der Waals	Light green fill	PHE A:140, PHE A:146, LEU A:95, ASN A:338, GLY A:238, PHE A:234, ILE A:287, TYR A:346, LEU A:299, VAL A:185
	Conventional Hydrogen Bond	Bright green dashed lines	ASP A:342, SER A:143, LEU A:145
	Unfavorable Acceptor-Acceptor	Red fill + red dashed lines	VAL A:139, LEU A:142, GLY A:141
	Pi-Sigma	Violet fill	LEU A:145
	Pi–Pi Stacked	Pink fill	TRP A:295
	Pi-Alkyl	Light pink fill	**ALA A:148**
E279K + Ganomycin-I	Van der Waals	Light green fill	VAL A:290, ASN A:338, **GLN A:339**, PHE A:140, PHE A:146, ILE A:147, VAL A:185, THR A:138, PHE A:188
	Unfavorable Bump	Red fill + red dashed lines	SER A:143, SER A:144, LEU A:145, LEU A:142, GLY A:141, PHE A:234, ASP A:342, LEU A:291
	Pi-Alkyl	Light purple/pink fill	**ALA A:148**
T277M + G-Mangostin	Van der Waals	Light green fill	SER A:143, SER A:144, PHE A:146, GLY A:238, PHE A:234, LEU A:237, ASP A:99, ASN A:338, **GLN A:339**

	Unfavorable Bump	Red fill + red dashed lines	PHE A:140, VAL A:139, THR A:138, MET A:137, GLY A:141, LEU A:142, LEU A:145, ASP A:342, LEU A:291
	Carbon Hydrogen Bond	Gray solid line	TRP A:295
	Pi–Pi T-shaped	Bright pink dashed lines	TRP A:295
	Pi-Alkyl	Light pink fill	**ALA A:148**, LEU A:95
T277M + Luteolin	Van der Waals	Light green fill	ILE A:287, TYR A:346, LEU A:95, ASN A:338, PHE A:140, PHE A:146, PHE A:234, LEU A:299, VAL A:185, GLY A:238
	Unfavorable Bump	Red fill + red dashed lines	VAL A:139, LEU A:142, GLY A:141, LEU A:291
	Conventional Hydrogen Bond	Bright green dashed lines	ASP A:342, SER A:144, LEU A:145, THR A:138
	Pi-Sigma	Violet fill	LEU A:145
	Pi–Pi Stacked	Pink fill	TRP A:295
	Pi-Alkyl	Light pink fill	**ALA A:148**
T277M + Proflavine	Van der Waals	Light green fill	LEU A:95, ASN A:338, PHE A:140, VAL A:139, PHE A:234
	Unfavorable Bump/Acceptor-Acceptor	Red fill + red dashed lines	ASP A:342, SER A:144, GLY A:141, LEU A:142, LEU A:145, SER A:143, LEU A:291, TRP A:295
	Conventional Hydrogen Bond	Bright green dashed lines	THR A:138
	Unfavorable Donor-Donor	Solid red line	–
	Pi-Alkyl	Light pink fill	**ALA A:148**

4. DISCUSSION

Worldwide, genome-wide association studies (GWAS) have greatly advanced our knowledge of the genetic factors involved in ocular inflammatory diseases such as conjunctivitis, by identifying susceptibility loci and genetic variants associated with disease development and progression [53]. Single nucleotide polymorphisms (SNPs) represent the most ubiquitous form of genetic variation in the human genome, characterized by the replacement of a single nucleotide at a defined genomic position. While most SNPs are functionally neutral, those situated within coding sequences, regulatory elements, or splice sites can exert considerable biological effects by modifying protein conformation, altering gene expression levels, or disrupting mRNA processing [54, 55]. In conjunctivitis, SNPs within genes implicated in immune modulation, inflammatory pathways, and epithelial barrier maintenance have been associated with increased susceptibility to both infectious and allergic forms of the disease [56, 57]. Furthermore, certain SNPs can enhance or suppress the expression of pro-inflammatory cytokines, alter receptor sensitivity, or affect immune cell signaling pathways, thereby modulating the severity and duration of the inflammatory response [58]. For example, variants in **FOXP3** (rs3761548) and **GATA3** (rs1269486) have been implicated in the exaggerated Th2 immune responses commonly observed in allergic conjunctivitis, influencing T-cell function and cytokine production [59, 60]. Subsequently, SNPs within the **PTGER3 (rs1327464),** have been associated with heightened ocular inflammation and linked to severe drug-induced hypersensitivity syndromes such as Stevens–Johnson syndrome when co-occurring with specific HLA alleles [15].

These genetic variations not only contribute to interindividual differences in disease susceptibility but also have implications for drug responsiveness. The identification and functional characterization of disease-associated SNPs through GWAS and bioinformatics analysis provide critical insights into the molecular mechanisms of conjunctivitis and pave the way for the development of personalized therapeutic interventions. This study aims to comprehensively explore the impact of SNPs in the *PTGER3* gene on the structure and function, which is implicated in conjunctivitis. By employing a range of computational pathogenicity prediction tools, the study pursues to identify deleterious mutations that could disrupt receptor activity. Further, through three-dimensional protein modeling and molecular docking analyses, the research will assess that genetic variations affect ligand binding sites and provide a foundation for integrating genetic data with functional analyses, thereby advancing personalized approaches for diagnosis and targeted treatment in ocular inflammatory diseases.

The *PTGER3* gene encodes the EP3 receptor, one of the four subtypes of prostaglandin E_2 (PGE_2)

receptors, and is a critical mediator of inflammatory responses within various tissues, including the ocular surface through its involvement in the PGE_2 signaling cascade [61]. Upon binding to its ligand, the EP3 receptor primarily couples with inhibitory G proteins (Gi), leading to a reduction in intracellular cyclic adenosine monophosphate (cAMP) levels. This suppression of cAMP activates downstream signaling pathways that enhance vascular permeability, promote leukocyte infiltration, and stimulate the release of pro-inflammatory cytokines and chemokines. These molecular events collectively contribute to hallmark clinical symptoms of conjunctivitis, such as redness, edema, itching, and discomfort [62]. Notably, the *PTGER3* gene undergoes alternative splicing, resulting in multiple isoforms (EP3-1 to EP3-8), each possessing distinct intracellular signaling capabilities, which may influence the severity and progression of ocular inflammation [63-65]. The gene is abundantly expressed in ocular tissues including the conjunctival epithelium, corneal endothelium, and ciliary body, highlighting its local functional relevance [66].

The role of PTGER3 in conjunctival inflammation has not been thoroughly investigated despite its established involvement in systemic inflammatory processes. Investigating the effects of deleterious SNPs on the structure and function of the EP3 receptor may uncover new mechanisms contributing to individual susceptibility to conjunctivitis. Such insights could facilitate the development of EP3-targeted therapies and support personalized treatment approaches to control inflammation. PTGER3's alternative splicing generates multiple isoforms with varied intracellular signaling cascades, potentially affecting disease severity and progression. Moreover, integrating GWAS-derived genetic data with these bioinformatics methodologies holds promise for identifying genetically predisposed individuals and guiding the development of personalized, genotype-driven therapeutic interventions for ocular inflammatory disorders [67]. To examine the functional and structural consequences of PTGER3 gene variants, a robust computational approach was employed. The complete genomic sequence (RefSeq ID: NC_000001.11) and corresponding protein sequence (UniProt ID: P43115.1) were retrieved in FASTA format from the NCBI and UniProt databases, respectively. Data on SNPs were then compiled from a range of established genomic repositories, including dbSNP NCBI, Ensembl, and gnomAD, to ensure comprehensive coverage and diversity of the variant dataset.

Functional annotation and pathogenicity assessment of PTGER3 SNPs were carried out using a suite of bioinformatics tools. SNPnexus, PANTHER, PolyPhen-2, and PredictSNP were employed to evaluate evolutionary conservation and the likely functional consequences of the variants. To further discern disease-associated mutations, SNP&GO, Meta-SNP, and SuSPect were utilized, offering predictions grounded in protein function, ontology data, and interaction networks. Protein stability alterations due to amino acid substitutions were predicted using iStable and MUpro, which integrate sequence-based and structural parameters. The HOPE server was applied to interpret structural consequences, including changes in physicochemical properties, residue conservation, and domain-specific relevance. For structural modeling, the three-dimensional structure of PTGER3 was generated using SWISS-MODEL and refined via GalaxyRefine to enhance local accuracy and side-chain orientation. Model validation was conducted using ProSA-web and QMEAN scoring, alongside PROCHECK, ERRAT, and Verify3D which collectively assessed stereochemical quality, atomic interactions, and residue environments. Structural deviations between native and mutant forms were analyzed through TM-align and Missense3D. In molecular docking studies, candidate ligands were sourced from the PubChem and LOTUS databases. Active site identification was performed using FT Site, and docking simulations were executed in PyRx with energy-minimized protein structures. Protein–ligand interactions, including binding orientation and contact residues, were visualized and analyzed using BIOVIA Discovery Studio. This integrative computational pipeline provided first comprehensive insights into the potential structural and functional consequences of PTGER3 variants.

Our analysis identified 51 variants consistently predicted as deleterious by SNPnexus. PolyPhen-2 (HumVar) classified all these variants as probably damaging, while HumDiv corroborated 50 damaging variants, with only C14R considered benign. PredictSNP categorized 35 variants as deleterious and

16 as neutral, whereas PANTHER predicted 7 as possibly or probably damaging and labeled the remaining 44 as benign. Functional assessments using SNP&GO and SuSPect further identified 12 and 29 variants, respectively, as disease-associated. Meta-SNP supported the pathogenic potential of 30 variants. Evaluation of protein stability through MUpro indicated that 49 mutations decreased structural stability, with the exceptions of S126L and F132I, while iStable predicted 34 mutations to negatively impact the protein's structural integrity.

In addition, HOPE analysis prioritized 15 highly conserved and functionally detrimental mutations for advanced structural modeling assessment. The 3D structure of the PTGER3 was generated using AlphaFold-derived templates and underwent refinement to enhance local geometry and side-chain orientation. Model validation shows a high proportion of residues within favored regions of the Ramachandran plot and an ERRAT score above 96%, confirmed its suitability for downstream structural evaluations. Moreover, C358R, E279K, and T277M were particularly notable due to their predicted effects on protein architecture. Structural disruption analysis with Missense3D indicated that these mutations either interfered with buried hydrogen bond networks or caused substantial alterations in internal cavity volume. These changes are likely to destabilize the protein structure, potentially impairing normal signaling activity.

Molecular docking analyses of both wild-type and mutant PTGER3 receptors, supported by FTsite predictions, revealed three binding pockets with consistent ligand interactions. Compounds such as luteolin, proflavine, γ-mangostin, and ganomycin-I exhibited strong binding affinities, stabilized by van der Waals forces, hydrogen bonds, and π–π interactions. These ligands consistently engaged key residues including ALA148, LEU145, ILE287, THR138, and LEU299 which were also identified within the FTsite-predicted active pockets, reinforcing their significant in ligand stabilization. The overlap between docking interaction sites and predicted binding pockets highlights their relevance as therapeutic targets for PTGER3 modulation in ocular inflammatory disorders.

While the study provided detailed computational insights into PTGER3 mutations and their potential therapeutic targeting, several constraints must be acknowledged. A primary limitation lies in the exclusive reliance on in silico tools. Although such approaches offer valuable initial assessments, they are inherently predictive and must be substantiated through laboratory-based experimentation. Without empirical data, conclusions about mutation pathogenicity, structural alterations, and ligand efficacy remain hypothetical. Functional validation using receptor expression assays, ligand-binding affinity tests, and signaling response measurements in cellular or tissue-based systems would significantly enhance the credibility of the predictions. Moreover, several strategies can advance the findings of the present study. Experimental validation using site-directed mutagenesis, receptor overexpression, and downstream signaling analysis would establish causative links between specific mutations and altered receptor function. Integration of transcriptomic or proteomic profiles from conjunctivitis patients could help correlate variant presence with clinical phenotypes, providing a stronger basis for pathogenicity assessments In addition, adopting CRISPR/Cas9 gene editing to introduce specific PTGER3 mutations in cell lines or animal models would offer powerful systems for studying the physiological relevance of prioritized variants. These platforms could also serve as testbeds for evaluating the efficacy and specificity of candidate modulators. Finally, the development of structure-guided drug design pipelines, coupled with iterative molecular docking and dynamics simulations, could facilitate the synthesis of optimized ligands tailored to the unique structural features of mutant PTGER3 receptors. Such efforts would support the broader goal of personalized medicine for inflammatory ocular conditions.

CONCLUSION

This study provides the first comprehensive computational characterization of PTGER3 variants correlated with conjunctiva inflammation. By integrating multiple pathogenicity predictors, structural modeling, and molecular docking workflows, we identified fifteen high-risk SNPs that perturb receptor architecture and stability. Notably, the C358R, E279K, and T277M variants induce significant side-chain volume alterations and core

destabilization, underscoring their potential to disrupt ligand recognition and downstream signaling. FTSite-predicted binding pockets, confirmed by docking analyses, highlight key residues ALA148, LEU145, ILE287, THR138, and LEU299 essential for ligand engagement. Among the twelve screened compounds, Luteolin, G-Mangostin, and Proflavine exhibited robust binding to wild-type PTGER3, while mutant receptors displayed distinct interaction profiles that may confer differential drug sensitivity. These insights lay a foundation for structure-guided optimization of selective EP3 modulators and emphasize the need for experimental validation of the most promising variants and ligands. Ultimately, this in silico framework advances our understanding of genetic determinants in conjunctivitis and offers a strategic roadmap for the rational design of precision-targeted therapies.

Acknowledgment
No acknowledgments to declare.
Author Contributions
All authors contributed equally to the research and preparation of this manuscript.
Declaration
This work is original and has not been published or submitted elsewhere.
Conflict of Interest
The authors declare no conflict of interest.

REFERENCES

1. de Laet, C., et al., *Recommendations for the management of tyrosinaemia type 1.* Orphanet J Rare Dis, 2013. 8: p. 8.
2. Tariq, F., *Allergic Conjunctivitis: Review of Current Types, Treatments, and Trends.* Life (Basel), 2024. 14(6).
3. Azari, A.A. and A. Arabi, *Conjunctivitis: A Systematic Review.* J Ophthalmic Vis Res, 2020. 15(3): p. 372-395.
4. Shekhawat, N.S., et al., *Antibiotic Prescription Fills for Acute Conjunctivitis among Enrollees in a Large United States Managed Care Network.* Ophthalmology, 2017. 124(8): p. 1099-1107.
5. Oikonomakou, M.Z., et al., *Bacteriology and Antimicrobial Susceptibility Patterns of Childhood Acute Bacterial Conjunctivitis in Western Greece.* Med Hypothesis Discov Innov Ophthalmol, 2019. 8(4): p. 266-271.
6. Yeu, E. and S. Hauswirth, *A Review of the Differential Diagnosis of Acute Infectious Conjunctivitis: Implications for Treatment and Management.* Clin Ophthalmol, 2020. 14: p. 805-813.
7. Teklemariam, E., et al., *Bacterial profile and antimicrobial susceptibility patterns among patients clinically suspected of bacterial conjunctivitis at the ophthalmologic clinic of Jimma Medical Center, Southwest Ethiopia.* Frontiers in Tropical Diseases, 2025. Volume 6 - 2025.
8. Villegas, B.V. and J.M. Benitez-Del-Castillo, *Current Knowledge in Allergic Conjunctivitis.* Turk J Ophthalmol, 2021. 51(1): p. 45-54.
9. Irkec, M.T. and B. Bozkurt, *Molecular immunology of allergic conjunctivitis.* Curr Opin Allergy Clin Immunol, 2012. 12(5): p. 534-9.
10. Leonardi, A., et al., *Epidemiology of allergic conjunctivitis: clinical appearance and treatment patterns in a population-based study.* Curr Opin Allergy Clin Immunol, 2015. 15(5): p. 482-8.
11. Dupuis, P., et al., *A contemporary look at allergic conjunctivitis.* Allergy Asthma Clin Immunol, 2020. 16: p. 5.
12. Boghdady, W.A., et al., *Correlation between forkhead box P3 (rs3761548) gene polymorphism and serum interleukin13 as biomarkers of severity in Egyptian allergic conjunctivitis: a retrospective study.* Frontiers in Allergy, 2024. Volume 5 - 2024.
13. Marques, C.R., et al., *Genetic and epigenetic studies of FOXP3 in asthma and allergy.* Asthma Res Pract, 2015. 1: p. 10.
14. Ahmed, S.A.E., et al., *Association of GATA3 gene polymorphism with allergic conjunctivitis and allergic rhinitis.* Egyptian Journal of Medical Microbiology, 2022. 31(3): p. 117-124.
15. Ueta, M., et al., *HLA-A*02:06 and PTGER3 polymorphism exert additive effects in cold medicine-related Stevens-Johnson syndrome with severe ocular complications.* Hum Genome Var, 2015. 2: p. 15023.
16. Heussen, F.M., et al., *Non-ocular primary malignancies in patients with uveal melanoma: the Liverpool experience.* British Journal of Ophthalmology, 2016. 100(3): p. 356.

17. Sugimoto, Y. and S. Narumiya, *Prostaglandin E receptors.* J Biol Chem, 2007. 282(16): p. 11613-7.
18. De Keijzer, S., et al., *The Multiple Faces of Prostaglandin E2 G-Protein Coupled Receptor Signaling during the Dendritic Cell Life Cycle.* International Journal of Molecular Sciences, 2013. 14(4): p. 6542-6555.
19. Kotani, M., et al., *Structural organization of the human prostaglandin EP3 receptor subtype gene (PTGER3).* Genomics, 1997. 40(3): p. 425-434.
20. Jin, J., G.F. Mao, and B. Ashby, *Constitutive activity of human prostaglandin E receptor EP3 isoforms.* Br J Pharmacol, 1997. 121(2): p. 317-23.
21. Sotozono, C. and M. Ueta, *Updates on the ocular manifestations and treatment of SJS/TEN.* Allergology International, 2025. 74(3): p. 356-360.
22. Wang, X., et al., *The Prostaglandin E2-EP3 Receptor Axis Regulates Anaplasma phagocytophilum-Mediated NLRC4 Inflammasome Activation.* PLoS Pathog, 2016. 12(8): p. e1005803.
23. Nakamura, Y., et al., *Prostaglandin EP3 receptor-expressing preoptic neurons bidirectionally control body temperature via tonic GABAergic signaling.* bioRxiv, 2022: p. 2022.04.15.488488.
24. König, C., et al., *Prostaglandin EP3 receptor activation is antinociceptive in sensory neurons via PI3Kγ, AMPK and GRK2.* Br J Pharmacol, 2023. 180(4): p. 441-458.
25. Dayem Ullah, A.Z., N.R. Lemoine, and C. Chelala, *SNPnexus: a web server for functional annotation of novel and publicly known genetic variants (2012 update).* Nucleic Acids Res, 2012. 40(Web Server issue): p. W65-70.
26. Mi, H., et al., *PANTHER version 16: a revised family classification, tree-based classification tool, enhancer regions and extensive API.* Nucleic Acids Res, 2021. 49(D1): p. D394-d403.
27. Adzhubei, I.A., et al., *A method and server for predicting damaging missense mutations.* Nat Methods, 2010. 7(4): p. 248-9.
28. Waheed, S., et al., *Identification and In-Silico study of non-synonymous functional SNPs in the human SCN9A gene.* PLoS One, 2024. 19(2): p. e0297367.
29. Bendl, J., et al., *PredictSNP: robust and accurate consensus classifier for prediction of disease-related mutations.* PLoS Comput Biol, 2014. 10(1): p. e1003440.
30. Venkata Subbiah, H., P. Ramesh Babu, and U. Subbiah, *Determination of deleterious single-nucleotide polymorphisms of human LYZ C gene: an in silico study.* Journal of Genetic Engineering and Biotechnology, 2022. 20(1): p. 92.
31. Capriotti, E., R.B. Altman, and Y. Bromberg, *Collective judgment predicts disease-associated single nucleotide variants.* BMC Genomics, 2013. 14 Suppl 3(Suppl 3): p. S2.
32. Yates, C.M., et al., *SuSPect: enhanced prediction of single amino acid variant (SAV) phenotype using network features.* J Mol Biol, 2014. 426(14): p. 2692-701.
33. Chen, C.W., J. Lin, and Y.W. Chu, *iStable: off-the-shelf predictor integration for predicting protein stability changes.* BMC Bioinformatics, 2013. 14 Suppl 2(Suppl 2): p. S5.
34. Cheng, J., A. Randall, and P. Baldi, *Prediction of protein stability changes for single-site mutations using support vector machines.* Proteins, 2006. 62(4): p. 1125-32.
35. Venselaar, H., et al., *Protein structure analysis of mutations causing inheritable diseases. An e-Science approach with life scientist friendly interfaces.* BMC Bioinformatics, 2010. 11(1): p. 548.
36. Schwede, T., et al., *SWISS-MODEL: An automated protein homology-modeling server.* Nucleic Acids Res, 2003. 31(13): p. 3381-5.
37. Bilal, I., et al., *Homology Modeling and Structural Docking Analysis on a Human BDNF Gene by Using Computational Algorithms.* Journal of Advances in Biology & Biotechnology, 2025. 28(4): p. 464-487.
38. Heo, L., H. Park, and C. Seok, *GalaxyRefine: protein structure refinement driven by side-chain repacking.* Nucleic Acids Research, 2013. 41(W1): p. W384-W388.

39. Wiederstein, M. and M.J. Sippl, *ProSA-web: interactive web service for the recognition of errors in three-dimensional structures of proteins.* Nucleic Acids Res, 2007. 35(Web Server issue): p. W407-10.
40. Benkert, P., M. Biasini, and T. Schwede, *Toward the estimation of the absolute quality of individual protein structure models.* Bioinformatics, 2011. 27(3): p. 343-50.
41. Kabiraj, A., et al., *In silico comparative structural and functional analysis of arsenite methyltransferase from bacteria, fungi, fishes, birds, and mammals.* Journal of Genetic Engineering and Biotechnology, 2023. 21(1): p. 64.
42. Reyaz-Ahmed, A., R. Harrison, and Y.Q. Zhang. *3D protein model assessment using geometric and biological features.* in *The 2nd International Conference on Software Engineering and Data Mining*. 2010.
43. Ittisoponpisan, S., et al., *Can Predicted Protein 3D Structures Provide Reliable Insights into whether Missense Variants Are Disease Associated?* J Mol Biol, 2019. 431(11): p. 2197-2212.
44. Kim, S., et al., *PubChem in 2021: new data content and improved web interfaces.* Nucleic Acids Res, 2021. 49(D1): p. D1388-d1395.
45. Rutz, A., et al., *The LOTUS initiative for open knowledge management in natural products research.* Elife, 2022. 11.
46. Liao, J., et al., *In silico methods for identification of potential active sites of therapeutic targets.* Molecules, 2022. 27(20): p. 7103.
47. Yang, X. and A.A. Ivanov, *Computational structural modeling to discover ppi modulators.* 2020.
48. Dallakyan, S. and A.J. Olson, *Small-molecule library screening by docking with PyRx.* Methods Mol Biol, 2015. 1263: p. 243-50.
49. Visualizer, B.D.S., *Dassault Systemes; San Diego, CA, USA: 2021.* Version v21, 2021. 1: p. 20298.
50. Campolo, M. and I. Paterniti, *Antioxidants and Anti-Inflammatory Effects in Neurodegenerative Diseases (NDs).* Antioxidants, 2022. 11(6): p. 1172.
51. Lupak, M.I., et al., *[THE ALKALOID-FREE FRACTION FROM Galega officinalis EXTRACT PREVENTS OXIDATIVE STRESS UNDER EXPERIMENTAL DIABETES MELLITUS].* Ukr Biochem J, 2015. 87(4): p. 78-86.
52. García-Aranda, M.I., et al., *Anti-inflammatory effect and inhibition of nitric oxide production by targeting COXs and iNOS enzymes with the 1,2-diphenylbenzimidazole pharmacophore.* Bioorg Med Chem, 2020. 28(9): p. 115427.
53. Haines, J.L. and V.C. Sheffield, *The molecular genetics of eye diseases.* Hum Mol Genet, 2017. 26(R1): p. R1.
54. Vallejos-Vidal, E., et al., *Single-Nucleotide Polymorphisms (SNP) Mining and Their Effect on the Tridimensional Protein Structure Prediction in a Set of Immunity-Related Expressed Sequence Tags (EST) in Atlantic Salmon (Salmo salar).* Front Genet, 2019. 10: p. 1406.
55. Kashan, H.S., et al., *In silico analysis of Single Nucleotide Polymorphisms in human GCH1 gene.* Informatics in Medicine Unlocked, 2021. 27: p. 100808.
56. Hafez, R.A., et al., *Association of Interleukin 13 rs20541 Gene Polymorphism and Serum Periostin with Asthma and Allergic Conjunctivitis Among Egyptian Patients.* J Asthma Allergy, 2022. 15: p. 971-982.
57. Singh, N., et al., *Epithelial barrier dysfunction in ocular allergy.* Allergy, 2022. 77(5): p. 1360-1372.
58. Bhol, N.K., et al., *The interplay between cytokines, inflammation, and antioxidants: mechanistic insights and therapeutic potentials of various antioxidants and anti-cytokine compounds.* Biomedicine & Pharmacotherapy, 2024. 178: p. 117177.
59. Boghdady, W.A., et al., *Correlation between forkhead box P3 (rs3761548) gene polymorphism and serum interleukin13 as biomarkers of severity in Egyptian allergic conjunctivitis: a retrospective study.* Front Allergy, 2024. 5: p. 1437600.
60. Lu, Y., et al., *Expansion of CD4(+) CD25(+) and CD25(-) T-Bet, GATA-3, Foxp3 and RORγt cells in allergic inflammation, local lung distribution and chemokine gene expression.* PLoS One, 2011. 6(5): p. e19889.

61. Yan, S., et al., *Prostaglandin E(2) promotes hepatic bile acid synthesis by an E prostanoid receptor 3-mediated hepatocyte nuclear receptor 4α/cholesterol 7α-hydroxylase pathway in mice.* Hepatology, 2017. 65(3): p. 999-1014.
62. Haq, A., H. Wardak, and N. Kraskian, *Infective Conjunctivitis – Its Pathogenesis, Management and Complications*, in *Common Eye Infections*, I.A.A. Chaudhry, Editor. 2013, IntechOpen: Rijeka.
63. Rundhaug, J.E., et al., *The role of the EP receptors for prostaglandin E2 in skin and skin cancer.* Cancer Metastasis Rev, 2011. 30(3-4): p. 465-80.
64. Ricciotti, E. and G.A. FitzGerald, *Prostaglandins and inflammation.* Arterioscler Thromb Vasc Biol, 2011. 31(5): p. 986-1000.
65. Konya, V., et al., *E-type prostanoid receptor 4 (EP4) in disease and therapy.* Pharmacology & Therapeutics, 2013. 138(3): p. 485-502.
66. Ueta, M., et al., *Prostaglandin E receptor subtype EP3 expression in human conjunctival epithelium and its changes in various ocular surface disorders.* PLoS One, 2011. 6(9): p. e25209.
67. Alsaedi, S., et al., *AI-powered precision medicine: utilizing genetic risk factor optimization to revolutionize healthcare.* NAR Genom Bioinform, 2025. 7(2): p. lqaf038.